termis.

Tissue Engineering
& Regenerative Medicine
International Society

Engineered Heart Slice Model of Arrhythmogenic Cardiomyopathy Using Plakophilin-2 Mutant Myocytes

Adriana Blazeski, PhD,* Justin Lowenthal, BS,* Yin Wang, MD, PhD, Roald Teuben, BS, Renjun Zhu, PhD, Sharon Gerecht, PhD, Gordon Tomaselli, MD, and Leslie Tung, PhD

Arrhythmogenic cardiomyopathy (AC), a cause of sudden cardiac death among young and otherwise healthy individuals, is a heritable disease that can be modeled *in vitro* using patient-specific cardiac myocytes (CMs) from induced pluripotent stem cells. An understanding of underlying disease mechanisms, particularly in the early concealed stages, could lead to new diagnosis and treatment strategies. However, multicellular syncytial models are needed to understand how genetically encoded mutations of the desmosomes that interconnect cells lead to aberrant electrical conduction and arrhythmias. In this study, engineered heart slices (EHS) were created by seeding human induced pluripotent stem cell-derived CMs from an AC patient with a plakophilin-2 (*PKP2*) mutation onto intact slices of decellularized myocardium and then compared to age-matched AC CMs cultured as monolayers. After 2 weeks of culture, EHS developed into a confluent multilayered syncytia that exhibited spontaneous coordinated beating and could be electrically paced at cycle lengths ranging from 2000 to 500 ms. AC CMs cultured as EHS displayed highly aligned, dense, and ordered sarcomeric structures, with gene expression analyses revealing increased maturation. In addition, AC-relevant genes were affected by CM culture in EHS, with a substantial increase in *PPARG* and a decrease in *SCN5A* compared to monolayers. Functionally, AC EHS exhibited similar conduction velocities, shorter action potentials, and a slower and steadier spontaneous beat rate compared with monolayers. Reentrant arrhythmias could also be induced in AC EHS by S1-S2 pacing. Our findings suggest that the EHS microenvironment enhances the phenotype of AC CMs in culture while allowing for functional studies of an appropriately aligned syncytium of AC-CMs. Results reported here demonstrate the benefits of studying AC using EHS, a tissue construct that allows syncytial culture and the incorporation of matrix cues.

Keywords: cardiomyocyte, arrhythmogenic cardiomyopathy, induced pluripotent stem cells, engineered tissues, decellularized matrix, disease modeling

Impact Statement

Genetic heart diseases such as arrhythmogenic cardiomyopathy (AC), a common genetic cause of sudden cardiac death, can be modeled using patient-specific induced pluripotent stem cell-derived cardiac myocytes (CMs). However, it is important to culture these cells in a multicellular syncytium with exposure to surrounding matrix cues to create more accurate and robust models of the disease due to the importance of cell–cell and cell–matrix interactions. The engineered heart slice, constructed by seeding CMs on intact decellularized matrix slices, allows molecular and functional studies on an aligned multilayered syncytium of CMs. This study reveals the potential for an improved disease-in-a-dish model of AC.

Introduction

HUMAN INDUCED PLURIPOTENT stem cell-derived cardiac myocytes (hiPSC-CMs) have emerged as an attractive platform for disease modeling and drug testing, particularly for heritable cardiac diseases. Human tissue for the study of these diseases is not easily obtained and is limited to small samples from biopsies or whole organ samples that are not suitable for transplantation. As a result, our understanding of normal and diseased cardiac function has relied heavily on animal models.[1] Stem cell lines from patients suffering from ion channelopathies (such as long QT) and cardiomyopathies (such as familial

Department of Biomedical Engineering, Johns Hopkins University School of Medicine, Baltimore, Maryland.
*Both these authors contributed equally to this work.

dilated cardiomyopathy and catecholaminergic polymorphic ventricular tachycardia) have been created and can be used to interrogate disease effects on cellular electrophysiology, contractile function, structure, and expression of target genes.[2–5]

Multiple studies have demonstrated that such hiPSC-CMs, harboring the mutations of clinically diagnosed cardiac patients, recapitulate characteristic elements of disease phenotypes.[6] Along with the ability to recapitulate the disease on the cellular level, these cells can be made in large numbers to allow replicate experiments to be performed in genetically identical cells, making them suitable for high-throughput drug screening.[2]

One example of such a disease is arrhythmogenic cardiomyopathy (AC, also known as arrhythmogenic right ventricular dysplasia/cardiomyopathy, or ARVC, ARVD, ARVD/C). Estimates of the prevalence of AC range from 1 in 2000 to 1 in 5000,[7,8] and the disease commonly manifests during late childhood or adolescence.[9] It is found in 20% of individuals who experience sudden cardiac death (SCD)[10] and is the leading cause of SCD in young adults.[9] Along with frequent arrhythmias that can lead to SCD, AC is characterized by distinct histopathological features: right ventricular enlargement, loss of myocytes accompanied by inflammatory infiltrates, and replacement of lost myocardium with fibrous and fatty tissue that progresses from the subepicardium to the endocardium, leading to wall thinning and aneurysmal dilatation.[10,11] However, researchers have long been vexed by the early ''concealed'' stage of the disease, when electrical abnormalities have been observed in the absence of structural changes.

Genetic mutations have been identified in up to 60% of AC patients.[12] A majority of these mutations affect the proteins of desmosomes—cell–cell junctional complexes at the intercalated disc that interconnect adjacent CMs participate in a variety of signaling cascades and contribute (along with adherens junctions) to the relay of tensile force during contraction.[13] Mutations in five genes that encode components of the desmosome have been associated with AC: desmoplakin (*DSP*), desmocollin-2 (*DSC2*), desmoglein-2 (*DSG2*), plakophilin-2 (*PKP2*), and junctional plakoglobin (*JUP*).[8] Analysis of AC patient biopsy samples indicates the loss of desmosomes[11] and reduced levels of plakoglobin at the intercalated disc.[14]

Unlike biopsies that are fixed in time, hiPSC-CMs derived from AC patients could be used to study the pathogenic mechanisms of the disease, and several studies have demonstrated the ability of these cells to manifest a disease-like phenotype.[15–18] These studies hold promise for the investigation of underlying AC mechanisms, particularly in the early concealed stages of the disease. However, they have largely focused on single cell preparations. Syncytial models—models that allow cardiac cells to function as a ''single unit'' from a contractile and electrophysiologic standpoint—are needed to understand how genetically encoded mutations of the desmosomes that interconnect cells lead to aberrant electrical conduction and arrhythmias[19] and to develop new diagnosis and treatment strategies. Furthermore, preparations that reflect the structural and biophysical characteristics of the heart will be necessary to study tissue-level changes that accompany disease progression.

We have previously established an ''Engineered Heart Slice'' (EHS) model created from CMs seeded onto decellularized intact slices of extracellular matrix (ECM).[20] We believe that EHS is particularly well suited for enhancing and probing disease phenotypes that not only alter the syncytial behavior of cardiac cells but also may in turn be greatly influenced by the underlying ECM substrate. Because EHS incorporates the cardiac ECM and supports a functional syncytium of cardiac cells, we sought to establish its utility in modeling AC disease phenotype. In this study, we examine how the EHS microenvironment affects the electrophysiological and structural phenotype of AC hiPSC-CMs in comparison to monolayer models of the disease.

Methods

Genomic sequencing

Messenger RNA (mRNA) was isolated from samples of H9-CMs and AC-CMs using standard procedures using the TRIzol Reagent (Thermo Fisher Scientific, Waltham, MA) (further detail in the Supplementary Data; Supplementary Data are available online at www.liebertpub.com/tea). A portion of exon 3 of the *PKP2* gene was amplified by polymerase chain reaction (PCR) using the following primer sequences: CTGGCA TCAGAGCTCCTTCC (forward) and GTGGTCTGCCTCGAGCATAC (reverse). The resultant PCR products were sequenced.

Preparation of decellularized matrix slices

Hearts obtained from slaughterhouse pigs were rinsed in distilled and deionized water and stored overnight at −20°C. The following day, the hearts were allowed to thaw at room temperature for 1 h. A metal 8, 12, or 14 mm diameter punch was sterilized using 70% ethanol and used to punch out plugs of tissue from the left ventricle. These plugs were then sectioned into 300 μm thick slices parallel to the epicardium, and the slices were decellularized using a procedure modified from Ott *et al.*[21] After decellularization and washing were complete, slices were carefully handled with forceps, spread over plastic coverslips, and wrapped around the edges of the coverslip. Slices attached to coverslips were placed into a 24-well plate, immersed in phosphate buffered saline with antibiotics, and stored at 4°C until seeding (up to 2 weeks). Complete details for slice sectioning and decellularization are given in the Supplementary Data.

hiPSC differentiation and culture

H9 human embryonic stem cells (hESCs) and AC hiPSCs derived from a patient with a *PKP2* mutation (Supplementary Fig. S1) were cultured as cell monolayers and differentiated into CMs according to a slightly modified, previously published protocol.[22] Briefly, hESCs and hiPSCs were plated within wells of six-well culture plates coated with 1:200 Geltrex:DMEM/F-12 (Dulbecco's modified Eagle's medium/nutrient mixture F-12) with HEPES. For the first 22 h, hiPSCs were maintained in Essential 8 (E8) medium with 10 μM Y-27632 dihydrochloride (Tocris Bioscience, Bristol, United Kingdom). Afterward, hiPSCs were rinsed with DMEM/F-12 and fed with E8 medium every day. After 4 days of culture in E8, when the stem cells had reached about 80% confluence, differentiation was commenced (defined as day 0, or ''d0'' in the Supplementary Data). Spontaneous beating in the monolayers was observed starting at d7–9.

H9 hESC-CMs and AC hiPSC-CMs were seeded at d20 to make monolayers (for comparing H9 to AC) or at d30 after purification with glucose-free lactate-supplemented DMEM

for comparing AC monolayers to AC EHS. Cell culture dishes were coated with Geltrex and seeded at a density of 300,000 cells/cm^2 to make monolayers for immunostaining, western blot, or quantitative reverse transcription polymerase chain reaction (RT-PCR) analysis. Decellularized slices were seeded at a density of 900,000 cells/cm^2 to make H9 and AC EHS for contraction and mapping experiments. After seeding at d20 (for H9 vs. AC monolayer studies) or d30 (for AC monolayer vs. EHS studies), both monolayers and EHS were maintained in B27 with insulin for 14 days before evaluation on d34 or d44, respectively.

Characterization of monolayers using immunostaining, quantitative RT-PCR, and Western blot

To immunostain for cellular proteins, EHS were permeabilized with cold 0.5% Triton X-100, blocked with 10% goat serum, and incubated overnight in primary antibodies (1:200 in antibody diluent, antibodies listed and protocol detailed in the Supplementary Data). The following day, thorough washes with tris-buffered saline with 0.1% Tween 20 (TBS-T) were followed by staining with Nile Red and conjugated secondary antibodies Alexa Fluor 488, 568, and 633 (1:200; Invitrogen). Samples were stained with 4′,6-diamidino-2 phenylindole, dihydrochloride (DAPI), washed with TBS-T, and mounted on glass slides for confocal imaging.

Quantitative RT-PCR was performed on H9-CM and AC-CM monolayers after mRNA was extracted (methods described in the Supplementary Data). Reverse transcription was performed to create complementary DNA (cDNA) with the PCR Master Mix Kit (Thermo Fisher Scientific), using the MyGo Mini PCR system Azura Genomics Inc., Raynham, MA. RT-PCR was performed on each target in triplicate, using the primers detailed in Supplementary Table S1.

For protein analysis using western blot, cells were lysed with RIPA buffer (Thermo Fisher Scientific) supplemented with protease inhibitor (Sigma-Aldrich Corp., St. Louis, MO) and phosphatase inhibitor cocktail (Sigma-Aldrich Corp.) at study end points. All lysates were centrifuged at 12,000 g for 15 min at 4°C. Total protein was quantified with a Pierce BCA assay (Thermo Fisher Scientific). Thirty micrograms of protein lysates were resolved on 4–12% mini Bis-Tris gels (Bio-Rad, Hercules, CA) and transferred onto PVDF membranes for immunoblotting. Membranes were incubated with primary antibodies (listed in the Supplementary Data) overnight at 4°C. Secondary antibodies (1:20,000, goat anti-rabbit or mouse; LI-COR, Lincoln, NE) were used and imaged by Odyssey CLX (LI-COR) as per the manufacturer's protocol.

Protein band intensities were quantified and normalized to GAPDH band intensities using ImageJ software (NIH). Further details are provided in the Supplementary Data.

Beat rate studies

Videos of ∼1 cm^2 regions of monolayers and EHS were taken in a cell culture incubator using a Lumascope 720 microscope (Etaluma, Carlsbad, CA). Recordings were taken at 20–25 frames per second and analyzed using custom MATLAB scripts (described in the Supplementary Data) to extract beat rate from each sample. Each sample was evaluated at 7- and 14-day postseeding (d27 and d34 for monolayer studies, d37 and d44 for monolayer/EHS comparison), with 30 s videos taken every hour for 24 h.

Electrophysiological studies

EHS were stained with 10 μM of the voltage-sensitive dye di-4-ANEPPS (Sigma-Aldrich Corp.) in Tyrode's solution for 10 min at 37°C. Afterward, EHS were rinsed twice with Tyrode's and placed in a 35 mm dish filled with Tyrode's and 10 μM of the contraction inhibitor blebbistatin (Sigma-Aldrich Corp.). This dish was set on a stage heated to 37°C and allowed to equilibrate for at least 5 min. Samples were point paced with at least 30 stimulus pulses over a range of cycle lengths, starting from 2000 ms and decreasing until samples lost pace capture. EHS were optically mapped during pacing using a 100 × 100 pixel CMOS (complementary metal oxide semiconductor) camera (MiCAM Ultima-L; SciMedia, Costa Mesa, CA). Optical mapping data were analyzed using custom MATLAB scripts (described fully in the Supplementary Data).

To initiate reentry, EHS were paced using an S1-S2 protocol. A line electrode parallel to the ECM fibers was used to pace EHS at either 2000 or 1500 ms for 30 beats. Following the last pulse of this train of stimuli (S1), a premature stimulus (S2) was applied using a point electrode. The coupling interval between S1 and S2 was initially set to 600 ms and decreased in 10 ms steps until reentry was observed or S2 no longer elicited a response. Some samples were incubated in 100 μM carbenoxolone for 7 min before pacing.

Statistics

All data are presented as mean ± standard deviation (SD). Unpaired, unequal variance t-tests were performed for western blot and optical mapping analyses. Beat rate analysis data were analyzed using analysis of variance with Tukey's *post hoc* test for multiple comparisons.

Results

AC hiPSC-CMs recapitulate the disease phenotype on a cellular level

CMs differentiated from AC hiPSC-CMs were confirmed to carry a mutation in the *PKP2* gene,[15] as has been previously reported. Sanger sequencing of the portion of exon 3 of *PKP2* indicated a heterozygous insertion of thymine (T) between positions 971 and 972 (c.971_972InsT). This causes a frame shift starting with amino acid 324 and ending with an early stop codon at position 335 (A324fs335X/N) that results in a truncated protein (Supplementary Fig. S1). This mutation was not present in control H9 hESC-CMs (Supplementary Fig. S1).

To study whether AC-CMs could recapitulate some of the electrical and structural characteristics of the disease and model the early "concealed" stage, hiPSC-CMs were cultured as monolayers and compared to control monolayers of H9 hESC-CMs. Control and AC monolayers were prepared using the same seeding densities, substrates (a two-dimensional [2D] tissue culture treated surface coated with Geltrex), and maintained in culture for 2 weeks. These samples were then immunostained for plakoglobin, a desmosomal protein whose expression level, cellular localization, and signaling have been associated with AC. While both control and AC monolayers were made up of a dense population of CMs that stained positively for cardiac troponin I (cTnI), AC monolayers exhibited lower intensities of membrane-localized plakoglobin staining

(Fig. 1A), indicating that less of this protein is present at cell–cell junctions.

Nile Red stain was used to visualize lipid content in the monolayers and showed that AC monolayers had much more prevalent staining (greater lipid content) than H9 monolayers (Fig. 1B). H9 and AC monolayers expressed similar levels of β1, a prevalent integrin subunit, indicating a similar level of cell–matrix interaction (Fig. 1B).

Quantitative RT-PCR was used to further characterize and compare the gene transcripts of H9 and AC monolayers (Fig. 1C and Supplementary Table S1). When comparing expression of gene transcripts associated with ion channel proteins, AC monolayers exhibited moderate increases in *CACNA1C*, *HCN1*, and *KCNQ1*, moderate decreases in *HERG*, *KCNJ2*, and *SCN5A*, and larger (>0.5-fold) decreases in *CACNA1G*, *HCN4*, and *KCNA4* compared to expression of these transcripts in H9 monolayers. Assayed transcripts of calcium-handling proteins showed mixed effects of the AC phenotype. The expression of *ATP2A2* and *PLN* was greatly increased, expression of *RYR2* was only moderately increased, and expression of *CASQ2* was greatly decreased in AC-CMs. Furthermore, compared to H9-CMs, AC-CMs expressed decreased levels of desmosomal genes across the board, with moderately lower transcript levels of
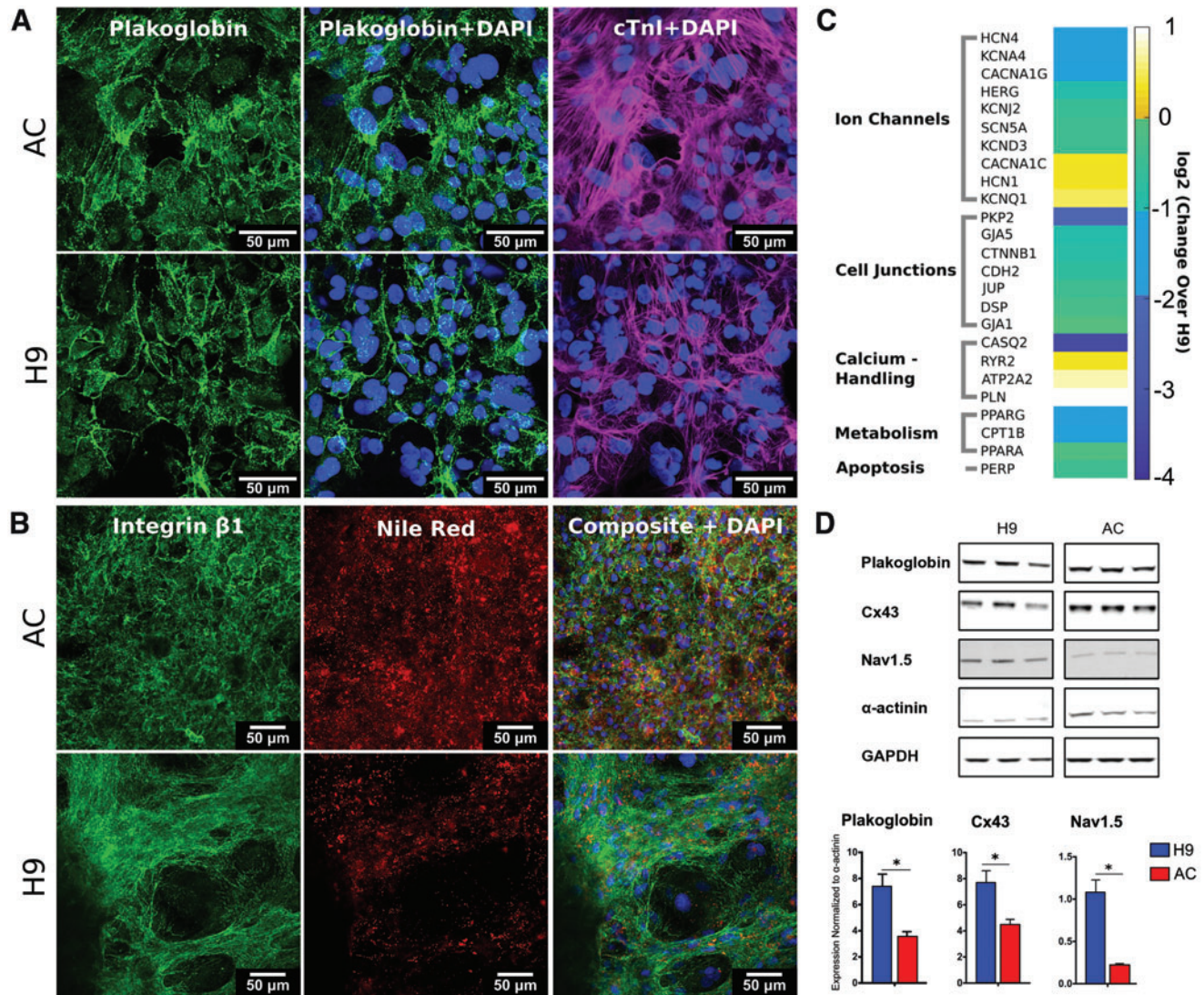

FIG. 1. Characterization of AC-CMs. AC-CMs (**A**, *top*) and H9-CMs (**A**, *bottom*) were stained for cardiac troponin I (*magenta*), plakoglobin (*green*), and DAPI (*blue*) to visualize myocytes. AC-CMs (**B**, *top*) and H9-CMs (**B**, *bottom*) were stained for integrin β1 (*green*), Nile Red (*red*), and DAPI (*blue*) to visualize matrix interactions and the presence of lipid droplets. Expression of mRNA transcripts associated with ion channels, cell junctional proteins, calcium-handling machinery, proteins involved in lipid metabolism, and apoptosis in AC-CM monolayers compared to that in H9-CM monolayers (**C**). Western blots of plakoglobin, Cx43, and Na$_V$1.5 in H9-CMs and AC-CMs (**D**). Expression of each protein was normalized to GAPDH (loading) and then to α-actinin and plotted for H9-CM monolayers (*blue bars*) and AC-CM monolayers (*red bars*). Error bars denote standard deviations. * Represents $p < 0.05$. $n = 3$ for each group. AC, arrhythmogenic cardiomyopathy; CMs, cardiac myocytes; DAPI, 4′,6-diamidino-2 phenylindole, dihydrochloride; mRNA, messenger RNA. Color images are available online.

CDH2, *CTNNB1*, and *GJA5* and substantially lower expression of *PKP2*.

Protein level expression of plakoglobin, Cx43, and Nav1.5 paralleled the gene transcript data, as expression of all three proteins was lower in AC-CMs than in H9-CMs (Fig. 1D, E) once normalized to the CM-specific structural protein α-actinin to account for differences in population purity (quantified in Supplementary Fig. S2).

Engineered heart slices enable dense cultures of AC hiPSC-CMs with high degrees of cellular alignment, structural order, robust junctional protein localization, and lipid droplets

While it was possible to assay changes in gene transcripts, proteins, and prevalence and localization of cellular components (through immunostaining) using 2D monolayer cultures, a more tissue-like preparation was needed to better assay contraction and the electrophysiological properties of a properly aligned syncytium. In addition, 2D tissue culture was found to have limited ability to maintain cardiac myocyte cell monolayers long term, which frequently aggregated or began to detach after 2 weeks of culture. To achieve a more robust preparation, AC-CMs were grown in EHS, which provided a supportive microenvironment. The decellularized matrix contains a mixture of ECM components that reflect the composition of native cardiac ECM and provides alignment cues for reseeded cells. Proteins critical to CM adhesion and maturation, such as laminin, were retained during decellularization without sacrificing the macrostructural collagen architecture (Fig. 2A).

After 2 weeks of culture on the EHS, AC-CMs demonstrated myofibril bundling and a high degree of alignment with the underlying matrix (Fig. 2B and Supplementary Videos S1 and S2, with matrix imaged using second harmonic generation to highlight collagen fibers). These cells organized into a multilayered syncytium. Alignment was much higher overall than in monolayers (Supplementary Fig. S3) and was more evident in cell layers closer to and within the surface topography of the ECM slice compared to layers farther from the ECM (Supplementary Figs. S3 and S4A and Supplementary Video S3). At high magnification, AC-CM myocytes were highly aligned with clear and ordered sarcomeric striations, and there was evidence of nuclear elongation and multinucleation in many cells (Fig. 2C).

Comparing monolayers to slices, cells and their respective nuclei were much larger in monolayers, most likely due to the flattening response of these cells to the high stiffness of the underlying coverslip and due to the higher density and tighter cell packing enabled by the EHS surface (Fig. 2D). Immunostaining of a variety of structural proteins (actinin and cTnI, a more mature isoform of troponin I) at lower and higher magnifications indeed demonstrated high degrees of structural alignment (Fig. 2C, D). Meanwhile, imaging of
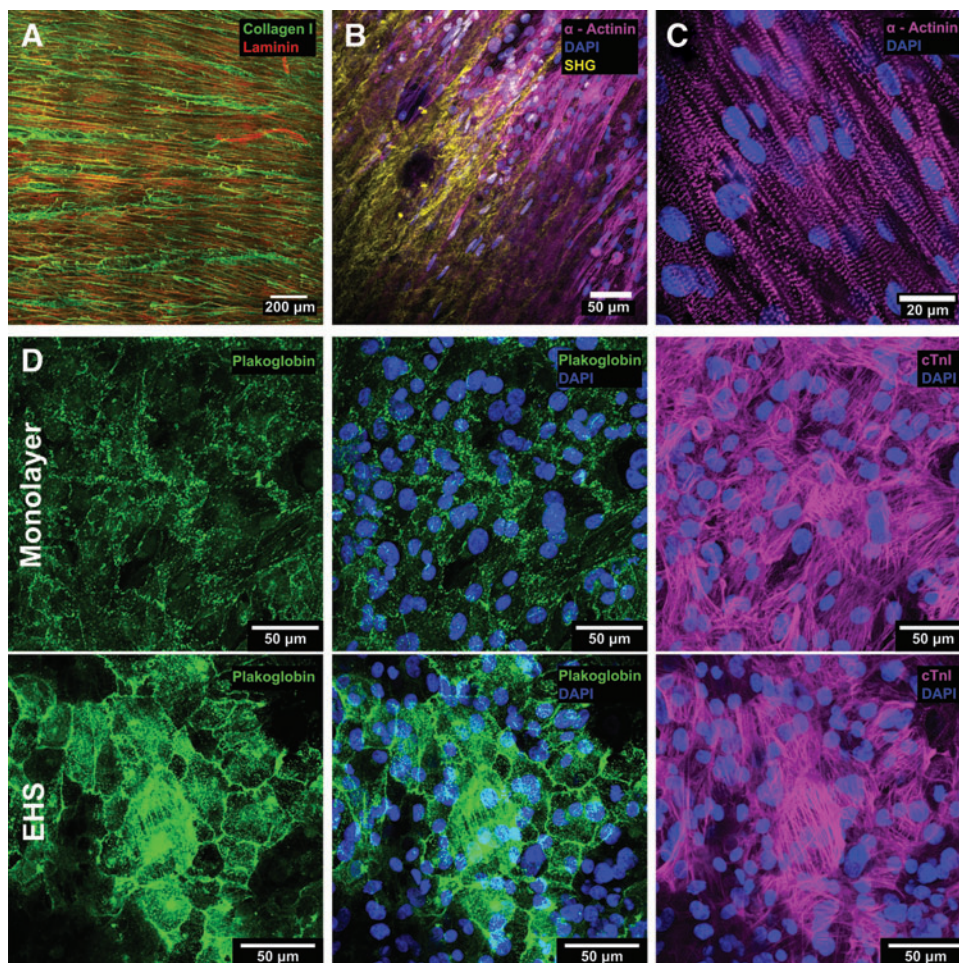

FIG. 2. Characteristics of AC EHS. Decellularized slices were stained for collagen I (*green*) and laminin (*red*) to illustrate the composition and arrangement of the extracellular matrix (**A**). Collagen fibers were visualized using second harmonic generation imaging (*yellow*), and AC-CMs were stained for α-actinin (*magenta*) and DAPI (*blue*) to illustrate the interaction between the cells and matrix in EHS (**B**). A higher magnification view of α-actinin and DAPI shows the orderly arrangement of sarcomeres in EHS (**C**). AC monolayers and EHS were compared (**D**) for staining for nuclei (*blue*), cTnI (*magenta*), and plakoglobin (*green*). All scale bars within (**D**) share the same value. cTnI, cardiac troponin I; EHS, engineered heart slice. Color images are available online.

the desmosomal protein plakoglobin, important to modeling AC, showed higher staining intensity overall and more cytoplasmic staining distribution in cells on EHS compared to those in monolayers (Fig. 2D, E). Staining of plakoglobin was robust in both preparations; although staining was often more diffuse and largely cytoplasmic in EHS, maximum intensity Z projections revealed a high degree of membrane localization in both preparations (Fig. 2D, E).

Finally, as demonstrated in monolayers (Fig. 1), EHS based on AC-CMs were positive for accumulated lipid and neutral fat droplets by staining with perilipin A and Nile Red, confirming that this aspect of the disease could also be visualized in EHS (Supplementary Fig. S4B, C).

AC-CMs show structural maturity, increased expression of ion channel and junctional genes, and altered expression of disease-relevant genes when cultured in EHS versus monolayers

Gene expression in EHS produced from AC-CMs was compared by quantitative PCR to that of batch- and age-matched AC-CMs seeded as 2D monolayers (Fig. 3). Structural genes often associated with CM maturation, *TNNI3* and *MYOM2*, were enhanced even as expression of *ACTN2* was significantly decreased. The latter finding may have been due to slight outgrowth of nonmyocytes on the EHS during 2 weeks of culture, as even lactate-treated AC-CMs were not 100% pure (Supplementary Fig. S2).

Ion channel genes *HCN1*, *HCN4*, *HERG*, and *KCNQ1* all saw moderate increases in expression in EHS, while *KCNJ2* was highly increased (Fig. 3). Meanwhile, *CACNA1C* and *CACNA1G* saw mild-to-moderate decreases, and *SCN5A* was also moderately decreased (Fig. 3). Expression of nearly all measured gap junction, desmosomal, and calcium handling genes saw mild-to-moderate increases in EHS over monolayer culture, although *CTNNB1* (gene coding for β-catenin) notably saw a mild decrease (Fig. 3). Finally, the metabolic gene *PPARG* was highly upregulated in EHS compared to monolayers (Fig. 3).

Altogether, these observations support previous data in our laboratory suggesting that EHS improves the maturity of hiPSC-CMs and mildly enhances the expression of many ion channel and junctional proteins. Indeed, major alterations to the latter proteins in our preparations seem to be in their localization rather than their gene expression. Importantly, the AC disease-relevant genes *PPARG* and *SCN5A* were substantially affected (*PPARG* up, *SCN5A* down) by culture in the EHS environment.

Engineered heart slices represent a syncytial model that can be used to investigate contractile and electrophysiological characteristics of AC hiPSC-CMs

When seeded onto decellularized slices to make EHS, AC-CMs began beating synchronously as early as 12 h later and nearly always after several days in culture. This coordinated beating persisted throughout 2 weeks in culture. On days 6 and 13 after seeding, 30-s videos of spontaneously beating EHS and monolayers were recorded once per hour for a consecutive 24-h period immediately after media replacement (Fig. 4A, B and Supplementary Video S4). These videos were processed to extract a trace representing the amplitude and time course of contraction (Fig. 4A, B),
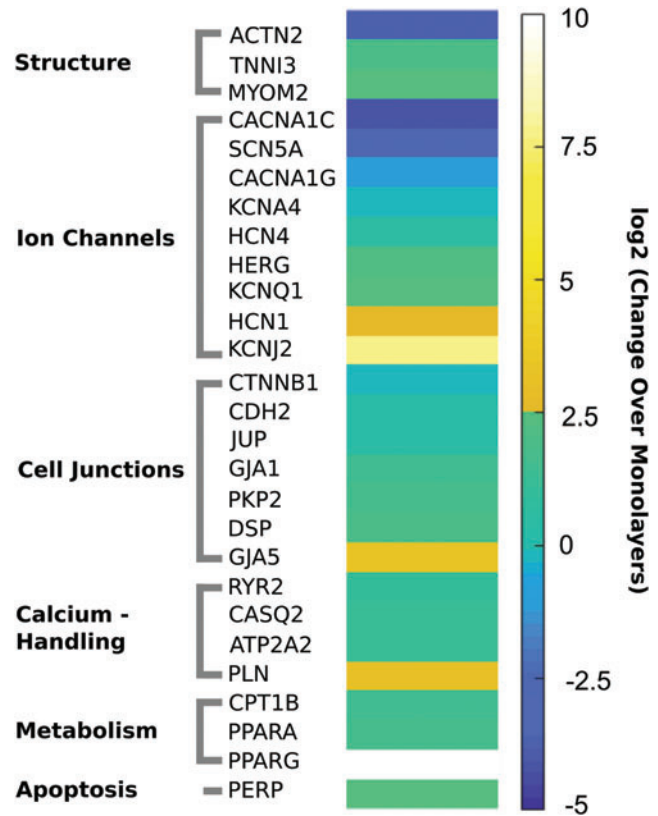

FIG. 3. Gene expression analysis of AC EHS. Expression of mRNA transcripts associated with structural proteins, ion channels, cell junctional proteins, calcium-handling machinery, proteins involved in lipid metabolism, and apoptosis in AC-CM EHS ($n=3$) compared to that in AC monolayers. Fold changes are visualized on a log scale. $n=3$ batches for EHS, $n=4$ batches for monolayers; each batch with three to eight replicates. Color images are available online.

which was then used to calculate the beat rate and variability (represented by the SD).

AC EHS showed consistently lower beat rates starting immediately after media change throughout the entire 24-h period, with the beat rate stabilizing at ~20 bpm (beats per minute) compared to an ~30 bpm rate for monolayers (Fig. 4C). Beat rate was significantly lower in EHS compared to monolayers at the end of both week 1 (21.1 ± 1.2 vs. 29.3 ± 3.4 bpm, respectively) and week 2 of culture (17.8 ± 2.0 vs. 27.6 ± 4.8 bpm, respectively), with the average beat rate in the EHS samples decreasing at week 2 compared to week 1 (Fig. 4D). Beat rates in EHS were also less variable compared to monolayers over the course of the 24-h period and when comparing individual EHS samples to one another, as represented by the size of the error bars (Fig. 4C, D).

The electrophysiological properties of EHS were compared to batch- and time-matched monolayers by optically mapping preparations after 2 weeks in culture, using point pacing at cycle lengths ranging from 2000 to 500 ms. Both EHS and monolayers exhibited smooth propagation of action potentials throughout the entire preparation (Fig. 5A and EHS in Supplementary Video S5, monolayer in Supplementary Video S6). Furthermore, for EHS there was evidence of anisotropic propagation in the elliptical shapes
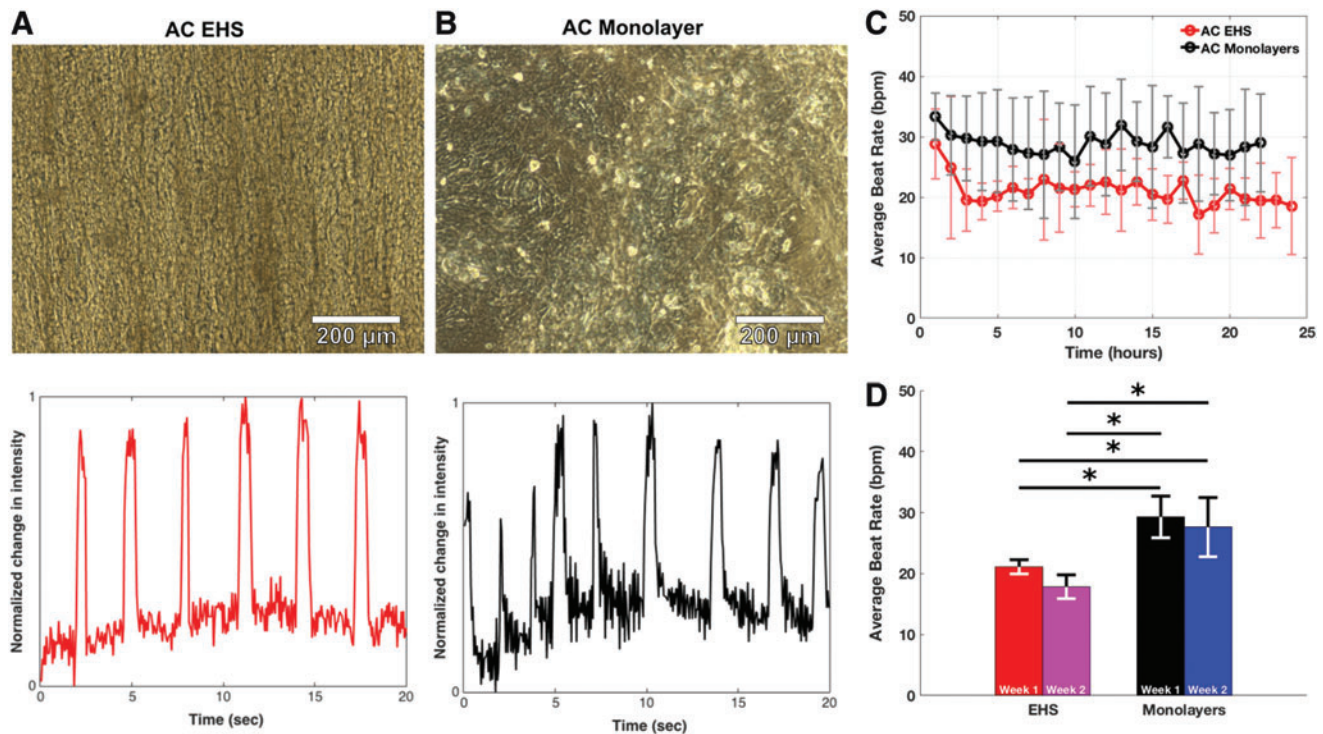
FIG. 4. Beat rate in AC EHS and AC monolayers. Example images (*top*) and traces (*bottom*) for AC EHS (**A**) and AC monolayers (**B**). Average beat rate for EHS (*red trace*) and monolayers (*black trace*) over a period of about 24 h measured 1 week after EHS and monolayer seeding (**C**). Comparison of average 24-h beat rates between EHS and monolayers measured 1 and 2 weeks after seeding (**D**). Error bars denote standard deviations. * Represents $p < 0.05$ (ANOVA with Tukey's *post hoc* test for multiple comparisons). $n = 11$ for EHS and $n = 18$ for monolayers. ANOVA, analysis of variance. Color images are available online.

of the propagation wavefront (Supplementary Video S5) and the isochrones in the conduction maps, whereas monolayers had isotropic propagation with more circular wavefronts and isochrones. EHS had faster conduction (greater spacing between isochrones) in the longitudinal direction of the matrix fibers (the vertical direction in Fig. 5A) and slower conduction in the transverse direction perpendicular to the matrix fibers.

Recordings of action potentials in monolayers and EHS revealed similar AP shapes in both preparations (Fig. 5B) and conduction velocities that were not statistically different at any pacing cycle length, ranging from 8.6 ± 1.6 to 5.3 ± 1.0 cm/s for EHS and 8.3 ± 1.1 to 6.3 ± 1.5 cm/s for monolayers (Fig. 5C). However, action potential duration, measured at 80% repolarization (APD_{80}), was significantly shorter in EHS at all measured cycle lengths except at 2000 and 500 ms and varied from 360.8 ± 10.4 to 266.0 ± 2.7 ms for EHS and 411.7 ± 20.2 to 302.1 ± 20.2 ms for monolayers across the range of pacing cycle lengths (Fig. 5D).

Finally, the ability to initiate reentrant activity in EHS was ascertained by applying a train of S1 stimuli at 2000 or 1500 ms cycle length from a line electrode followed by a premature S2 stimulus from a point electrode at the middle of the EHS (Fig. 6). By decreasing the timing interval between S1 and S2, reentry could be initiated consistently in our EHS preparations, including for at least 1 cycle in 7 out of 11 EHS samples (Fig. 6 and Supplementary Video S7). In addition, the application of carbenoxolone, a gap junctional blocker, in conjunction with the S1-S2 pacing protocol re-

sulted in sustained reentry in one EHS (Supplementary Fig. S5 and Supplementary Video S8).

Discussion

The AC line used in these studies was previously reported and characterized by Caspi *et al.*[15] We have confirmed in multicellular monolayers several major observations reported by Caspi *et al.* in single cells regarding the cellular phenotype of these AC-CMs: reduced expression of *PKP2* but no significant changes in *JUP* and *DSP*, diminished protein-level expression and membrane localization of plakoglobin and Cx43, and the presence of lipid droplets (a cellular-level pathophysiologic hallmark of AC). The reduction in and translocation of plakoglobin may represent a particularly reliable hallmark of the disease, as it has been suggested that it is a common pathway for AC, even in variants where the mutation is not in the plakoglobin gene.[14,16]

One prevalent hypothesis is that when plakoglobin fails to localize at the desmosome and instead redistributes to the nucleus, as is the case in AC, it can inhibit the Wnt-β catenin signaling pathway and increase the expression of fibrogenic and adipogenic genes.[11,23,24] In addition to decreased expression of plakoglobin, Caspi *et al.* noted the presence of lipid droplets in a third of their AC cells. While we did not differentiate between individual cells in our study, we noted that the overall Nile Red staining was greater in AC monolayers than in H9 monolayers. Furthermore, our findings that *CTNNB1* was reduced in AC-CMs
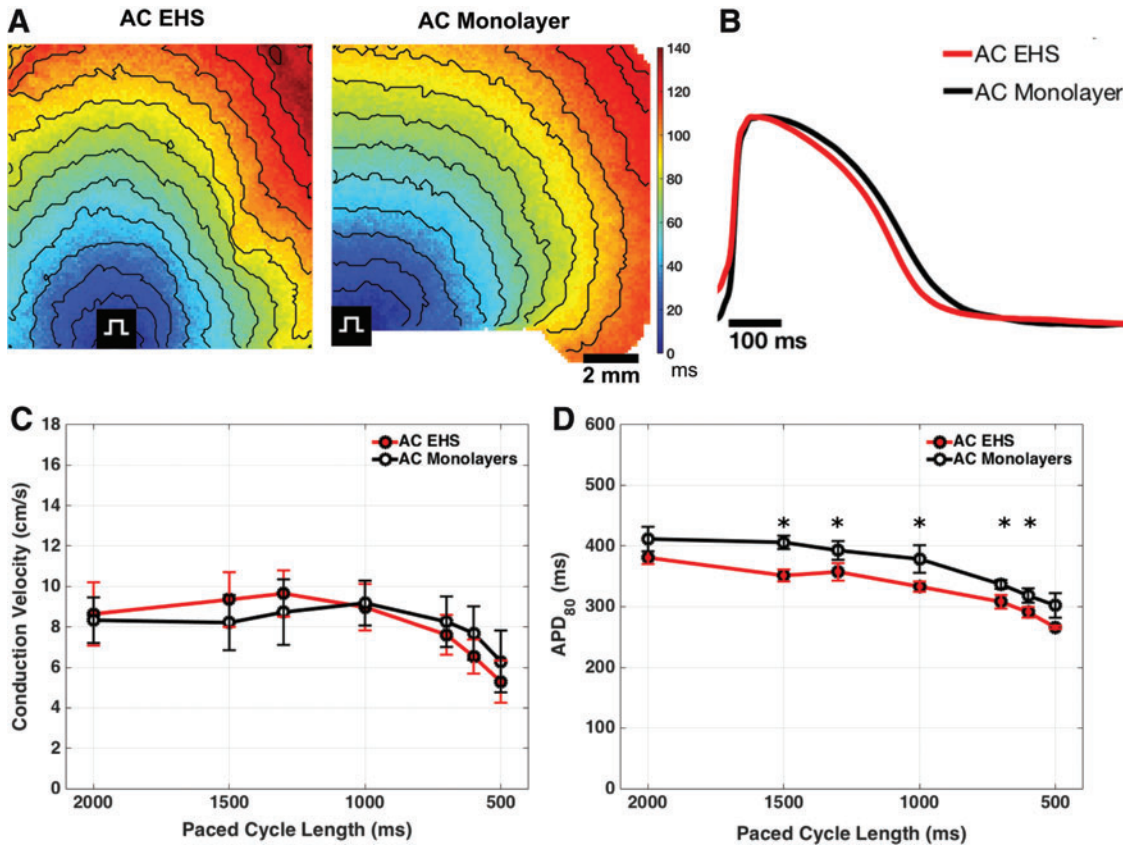
FIG. 5. Wavefront propagation in AC EHS and AC monolayers. Sample activation maps illustrate propagation of action potentials in an AC EHS (**A**, *left*) and AC monolayer (**A**, *right*) paced at 1300 ms cycle length. *Black lines* indicate isochrones at 10 ms intervals, and rectangular symbols indicate the pacing sites. Spatially averaged action potential traces are shown for EHS (**B**, *red trace*) and monolayer (**B**, *black trace*) paced at 1300 ms cycle length. Conduction velocities (**C**) and APD$_{80}$ (**D**) at different pacing rates are plotted for EHS (*red traces*) and monolayers (*black traces*). Error bars denote standard deviations. $n = 2-8$ for AC EHS and $n = 4-8$ for AC monolayers. * Denotes $p < 0.05$ when comparing EHS with monolayers. APD$_{80}$, action potential duration, measured at 80% repolarization. Color images are available online.

mirror the report of reduced β-catenin protein density in the Caspi study.

While other groups have performed immunolabeling, gene, and protein expression studies of AC hiPSC-CMs, functional implementations of AC-CM syncytia have been lacking. It is important for diseases such as AC that they be studied in syncytial preparations, as they depend on cell–cell interactions, and their electrophysiologic and histopathologic manifestations at the tissue level may not be evident in single cells. Structural proteins in adhesive junctions such as plakoglobin (also known as γ-catenin) can also function as signaling molecules, leading to the prevalent hypothesis that the AC disease phenotype is a result of weakened cell–cell adhesion arising from mutations in desmosomal proteins. This weakness then promotes cell detachment and death, as well as inflammatory cell infiltration, especially during vigorous exercise when the mechanical demands on the heart are elevated, and subsequently leads to build up of fibrofatty tissue.[24] This fibrotic infiltrate can then serve as a substrate for reentrant arrhythmias.

Another proposed pathogenic mechanism stems from the observation that desmosomes, gap junctions, and voltage-gated sodium channels have physical proximity and form a "triad" complex in the intercalated disc.[25] Reduction in plakoglobin may then be accompanied by reductions in both

Cx43 and Na$_V$1.5 expression,[26] gap junctional remodeling,[27] and reductions in I_{Na} and I_{K1} currents,[28–30] all of which could contribute to increased arrhythmia vulnerability.[26,28] Therefore, the remodeling of mechanical and electrical junctions between cells that is characteristic of AC necessitates the use of syncytial *in vitro* models of the disease if tissue-level arrhythmia such as reentry is to be understood.

To this end, we used our EHS platform to culture AC-CMs as a syncytium, which we could then use to characterize the gene and protein expression of these cells as populations and to measure a variety of functional properties: contraction and beat rate characteristics, conduction velocity (CV), APD, and propensity for reentrant arrhythmia. AC-CMs cultured as EHS for 2 weeks exhibited dense packing, a high degree of alignment, structurally ordered sarcomeres, robust membrane-localized desmosomal proteins, and evidence of lipid droplet accumulation. Comparison of gene expression of AC-CMs on EHS versus monolayers showed mildly increased structural and electrophysiologic maturity, a substantial increase in the metabolic gene *PPARG*, and a substantial decrease in *SCN5A* (the gene coding for Na$_V$1.5, a subunit of the voltage-gated sodium channel).

When we quantified the evolution and variability of beat rate over time in culture, we found lower and less variable beat rates in EHS compared to monolayers, a feature suggestive of
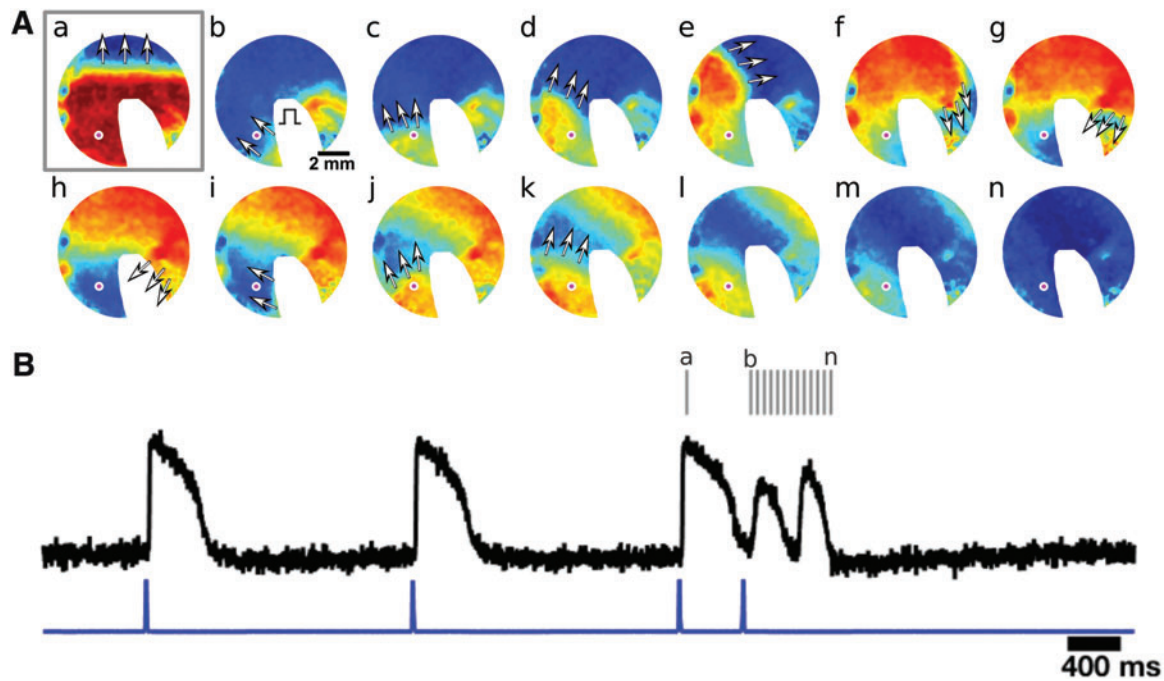
FIG. 6. Reentrant activity in AC EHS. Pacing with a line electrode from the bottom of the EHS at a cycle length of 2000 ms produced linear propagation of an activation wavefront across the EHS **(A.a)**. Pacing with a point electrode in the middle of the EHS, at a site indicated by the rectangular symbol, 480 ms after the last line electrode stimulus resulted in a clockwise spiral wave **(A.b–l)** that terminated after one rotation **(A.m, n)**. Voltage maps in **(A.b–n)** are 50 ms apart, and *white arrows* show local direction of the activation wavefront **(A)**. Area where electrode was placed is blanked out. The optical voltage recording throughout the time series is shown by the *black trace* in **(B)** for the location indicated by the *magenta dot* in **(A)**. The pacing pulses are indicated by the *blue trace*, and the time points of each snapshot **(A.a–n)** are indicated by the *gray tick marks* **(B)**. *White areas* are parts of the mapping field blocked from imaging by the S2 electrode. Color images are available online.

increased stability, consistency, and maturity of the model (with the caveat that beat rate is an imperfect readout of iPSC-CM and engineered tissue function/maturity). CV was comparable between AC EHS and monolayers, with both preparations having somewhat low absolute values (~ 8 cm/s at peak) compared to that expected in the adult ventricle. This observation is supported by the reduced gene expression and protein levels of Cx43 and $Na_V1.5$ in our preparations (Figs. 1 and 3), which is also reported in various models of AC compared to controls, leading to lower electrical coupling and suppressed conduction velocities.

However, unlike in monolayers, the three-dimensional topographical cues imparted by the matrix in EHS allowed cellular alignment and anisotropic conduction. APD was somewhat shorter in AC EHS than in AC monolayers, contrary to reports that APD is lengthened in AC hiPSC-CMs compared to healthy controls.[17] This discrepancy may arise from the fact that the cited study measured APD in single cells, whereas we used multicellular preparations which enable mechanical cell–cell interactions and, in the case of EHS, cell–matrix interactions. Finally, a novel aspect of our study is the observation of arrhythmogenic activity in EHS in the form of reentry. Hence, it may be possible to use EHS to study how the AC cellular phenotype results in aberrant multicellular electrical activity, such as that observed in the concealed stage of the disease.

Finally, our EHS platform offers several advantages for developing a disease model of AC. The biophysical and biochemical properties of the underlying matrix proteins can promote maturation and a more developed phenotype in AC-CMs. In addition, while AC has been conceptualized as a disease primarily affecting cell–cell cohesion,[31] changes in cell–matrix adhesion may also contribute to the pathological progression of the disease, especially given the cooperative balance between cell–cell and cell–matrix adhesions in the heart.[32] Thus, decellularized matrix is a particularly relevant microenvironment on which to culture AC-CMs and study their disease properties.

Furthermore, given that fibrosis and fat infiltration occur in AC, the secretion and digestion of matrix proteins must transpire during disease pathogenesis; culturing AC hiPSC-CMs in EHS with its ECM constituents presumably permits such actions to occur. We thus propose that EHS could lead to improved manifestation of this aspect of the disease phenotype *in vitro*. Finally, EHS are suited for future studies addressing how changes in mechanical properties or local ECM components affect the development of the disease. EHS can be created from different regions of the heart (such as from the right and left ventricles), from matrix of different ages, and from matrix that is engineered to be fibrotic, which when seeded with AC CMs can be used to study which matrix-level and cell-level factors lead to increased susceptibility to developing arrhythmia.

Disclosure Statement

None of the authors has any competing financial conflicts of interest to disclose.

Supplementary Material

Supplementary Data
Supplementary Figure S1
Supplementary Figure S2
Supplementary Figure S3
Supplementary Figure S4
Supplementary Figure S5
Supplementary Table S1
Supplementary Video S1
Supplementary Video S2
Supplementary Video S3
Supplementary Video S4
Supplementary Video S5
Supplementary Video S6
Supplementary Video S7
Supplementary Video S8

References

1. Hamlin, R.L. Animal models of ventricular arrhythmias. Pharmacol Ther **113,** 276, 2007.
2. Davis, R.P., van den Berg, C.W., Casini, S., Braam, S.R., and Mummery, C.L. Pluripotent stem cell models of cardiac disease and their implication for drug discovery and development. Trends Mol Med **17,** 475, 2011.
3. Zeevi-Levin, N., Itskovitz-Eldor, J., and Binah, O. Cardiomyocytes derived from human pluripotent stem cells for drug screening. Pharmacol Ther **134,** 180, 2012.
4. Blazeski, A., Zhu, R., Hunter, D.W., Weinberg, S.H., Zambidis, E.T., and Tung, L. Cardiomyocytes derived from human induced pluripotent stem cells as models for normal and diseased cardiac electrophysiology and contractility. Prog Biophys Mol Biol **110,** 166, 2012.
5. Zanella, F., Lyon, R.C., and Sheikh, F. Modeling heart disease in a dish: from somatic cells to disease-relevant cardiomyocytes. Trends Cardiovasc Med **24,** 32, 2014.
6. Sallam, K., Li, Y., Sager, P.T., Houser, S.R., and Wu, J.C. Finding the rhythm of sudden cardiac death: new opportunities using induced pluripotent stem cell-derived cardiomyocytes. Circ Res **116,** 1989, 2015.
7. Benjamin, E.J., Blaha, M.J., Chiuve, S.E., *et al.* Heart disease and stroke statistics-2017 update: a report from the American Heart Association. Circulation **135,** e146, 2017.
8. Basso, C., Bauce, B., Corrado, D., and Thiene, G. Pathophysiology of arrhythmogenic cardiomyopathy. Nat Rev Cardiol **9,** 223, 2012.
9. Saguner, A.M., Brunckhorst, C., and Duru, F. Arrhythmogenic ventricular cardiomyopathy: a paradigm shift from right to biventricular disease. World J Cardiol **6,** 154, 2014.
10. Murray, B. Arrhythmogenic right ventricular dysplasia/cardiomyopathy (ARVD/C): a review of molecular and clinical literature. J Genet Couns **21,** 494, 2012.
11. Corrado, D., Link, M.S., and Calkins, H. Arrhythmogenic right ventricular cardiomyopathy. N Engl J Med **376,** 61, 2017.
12. Orgeron, G.M., and Crosson, J.E. Arrhythmogenic right ventricular dysplasia/cardiomyopathy. Cardiol Young **27,** S57, 2017.
13. McCauley, M.D., and Wehrens, X.H.T. Animal models of arrhythmogenic cardiomyopathy. Dis Model Mech **2,** 563, 2009.
14. Asimaki, A., Tandri, H., Huang, H., *et al.* A new diagnostic test for arrhythmogenic right ventricular cardiomyopathy. N Engl J Med **360,** 1075, 2009.
15. Caspi, O., Huber, I., Gepstein, A., *et al.* Modeling of arrhythmogenic right ventricular cardiomyopathy with human induced pluripotent stem cells. Circ Cardiovasc Genet **6,** 557, 2013.
16. Ma, D., Wei, H., Lu, J., *et al.* Generation of patient-specific induced pluripotent stem cell-derived cardiomyocytes as a cellular model of arrhythmogenic right ventricular cardiomyopathy. Eur Heart J **34,** 1122, 2013.
17. Kim, C., Wong, J., Wen, J., *et al.* Studying arrhythmogenic right ventricular dysplasia with patient-specific iPSCs. Nature **7435,** 105. 2013.
18. Wen, J.-Y., Wei, C.-Y., Shah, K., Wong, J., Wang, C., and Chen, H.-S.V. Maturation-based model of arrhythmogenic right ventricular dysplasia using patient-specific induced pluripotent stem cells. Circ J **79,** 1402, 2015.
19. Sen-Chowdhry, S., Syrris, P., Ward, D., Asimaki, A., Sevdalis, E., and McKenna, W.J. Clinical and genetic characterization of families with arrhythmogenic right ventricular dysplasia/cardiomyopathy provides novel insights into patterns of disease expression. Circulation **115,** 1710, 2007.
20. Blazeski, A., Kostecki, G.M., and Tung, L. Engineered heart slices for electrophysiological and contractile studies. Biomaterials **55,** 119, 2015.
21. Ott, H.C., Matthiesen, T.S., Goh, S.-K., *et al.* Perfusion-decellularized matrix: using nature's platform to engineer a bioartificial heart. Nat Med **14,** 213, 2008.
22. Bhattacharya, S., Burridge, P.W., Kropp, E.M., *et al.* High efficiency differentiation of human pluripotent stem cells to cardiomyocytes and characterization by flow cytometry. J Vis Exp **(91),** 52010, 2014.
23. Delmar, M., and McKenna, W.J. The cardiac desmosome and arrhythmogenic cardiomyopathies: from gene to disease. Circ Res **107,** 700, 2010.
24. Saffitz, J.E., and Macrae, C.A. Mutations in desmosomal protein genes and the pathogenesis of arrhythmogenic right ventricular cardiomyopathy. Heart Rhythm **7,** 30, 2010.
25. Delmar, M. Desmosome–ion channel interactions and their possible role in arrhythmogenic cardiomyopathy. Pediatr Cardiol **33,** 975, 2012.
26. Noorman, M., Hakim, S., Kessler, E., *et al.* Remodeling of the cardiac sodium channel, connexin43, and plakoglobin at the intercalated disk in patients with arrhythmogenic cardiomyopathy. Heart Rhythm **10,** 412, 2013.
27. Asimaki, A., and Saffitz, J.E. Gap junctions and arrhythmogenic cardiomyopathy. Heart Rhythm **9,** 992, 2012.
28. Sato, P.Y., Musa, H., Coombs, W., *et al.* Loss of plakophilin-2 expression leads to decreased sodium current and slower conduction velocity in cultured cardiac myocytes. Circ Res **105,** 523, 2009.
29. Asimaki, A., Kapoor, S., Plovie, E., *et al.* Identification of a new modulator of the intercalated disc in a zebrafish model

of arrhythmogenic cardiomyopathy. Sci Transl Med **6,** 240ra74, 2014.

30. Cerrone, M., Noorman, M., Lin, X., *et al.* Sodium current deficit and arrhythmogenesis in a murine model of plakophilin-2 haploinsufficiency. Cardiovasc Res **95,** 460, 2012.

31. Hariharan, V., Asimaki, A., Michaelson, J.E., *et al.* Arrhythmogenic right ventricular cardiomyopathy mutations alter shear response without changes in cell–cell adhesion. Cardiovasc Res **104,** 280, 2014.

32. McCain, M.L., Lee, H., Aratyn-Schaus, Y., Kleber, A.G., and Parker, K.K. Cooperative coupling of cell-matrix and cell-cell adhesions in cardiac muscle. Proc Natl Acad Sci U S A **109,** 9881, 2012.

Address correspondence to:
Leslie Tung, PhD
Department of Biomedical Engineering
Johns Hopkins University
School of Medicine
720 Rutland Avenue, Traylor 703
Baltimore, MD 21205

E-mail: ltung@jhu.edu